Aggregation of Lipid A Variants: a Hybrid Particle-Field Model

Antonio De Nicola,[1,*] Thereza A. Soares,[2] Denys E. S. Santos,[2] Sigbjørn Løland Bore,[3] G. J. Agur Sevink,[4] Michele Cascella,[3] Giuseppe Milano[1]

[1]*Department of Organic Material Science, Yamagata University, Yonezawa 992-8510, Japan.*

[2]*Department of Fundamental Chemistry, Universidade Federal de Pernambuco, Cidade Universitária, Recife, PE 50740-560, Brazil*

[3]*Department of Chemistry and Hylleraas Centre for Quantum Molecular Sciences, University of Oslo, P.O. Box 1033, Blindern, 0315 Oslo, Norway*

[4]*Leiden Institute of Chemistry, Leiden University, P. O. Box 9502, 2300 RA Leiden, The Netherlands.*

Abstract

Lipid A is one of three components of bacterial lipopolysaccharides (constituting the outer membrane of Gram-negative bacteria) and is recognized to have an important biological role in inflammatory response of the immune system. Its biological activity is modulated by the number of acyl-chains and from the electrostatic interactions with the different counter-ions. In this paper we report a coarse-grained model of poly-acyl Lipid A based on the hybrid particle field molecular dynamics approach (hPF-MD). In particular, we investigate the stability of Lipid A bilayer with two different acyl-chains, hexa- and tetra-. We find a good agreement of the particle distribution along the cross-section of bilayer by comparing the density profiles calculated from hPF-MD simulations with respect to reference all-atom. Moreover, we validate the model simulating the self-assembly of lamellar phase from an initial random distribution of Lipid A/N^{2+} molecules in water. Finally, we test the stability of a vesicle composed of hexa-acylated Lipid A in water. The proposed model is able to maintain stable bilayer aggregates and spherical vesicle, and to correctly reproduce the phase behavior of Lipid A/Ca^{2+}/Water mixture.

1. Background

Lipopolysaccharides (LPS) are the major lipid constituents of the external leaflet of the asymmetric outer membrane (OM) in Gram-negative bacteria.[1,2] The OM acts as a structural and functional barrier against the penetration of xenobiotic agents like hydrophobic antibiotics, digestive enzymes, heavy metals, detergents, or bile salts.[3] The LPS molecule can contain three different regions: (i) the polymeric *O*-antigen (repetitive monosaccharide subunits) responsible for the bacterium immunospecificity,[4] (ii) a branched oligosaccharide brush (composed of 8-12 monosaccharide units) and (iii) Lipid A unit (composed by typically 4-6 acyl chains attached to a phosphorylated glucosamine disaccharide) responsible for the anchoring of the LPS leaflet onto the phospholipid leaflet of the OM.[5,6] Lipid A has a fundamental biological role as a stimulator of the inflammatory response by the immune system.[7–9] The immune response to the presence of Lipid A is modulated by variations of its chemical structure such as the number, length and position of acyl chains as well as by the overall molecular charge.[9–11]

The phase diagram of Lipid A in water includes four three-dimensional aggregation states: lamellar (L), hexagonal (H_I,) inverted hexagonal (H_{II}) and non-lamellar cubic (Q).[9,12] The relative stability of the different aggregation states depends on environmental conditions (pH, temperature, ionic strength, cation types) as well as on the chemical structure of Lipid A. It is understood that these parameters influence the Lipid A cross-section area of the hydrophobic section (the hydrocarbon chains) favoring the stability of a specific aggregation state.[9–11]

In the past decades, several MD studies have been reported on both LPS and Lipid A. In particular, all-atom[7,13–19] and coarse-grained (CG) models[5,20–23] have been developed and are continuously improved.[14,15,18] However, due to the time and length scale limits, simulations of large systems and/or phenomena occurring on time scales larger than the μs are still challenging even for CG models. Overcoming such bottlenecks may be achieved by the development of models for lipopolysaccharides within a density-functional approach,[24] and in particular by the hybrid particle-

field/molecular dynamics (hPF-MD) model.[25–27] The main advantage of hPF-MD is that the non-bonded pair interactions between particles are replaced by the evaluation of an external potential based on the local particle density. Thanks to an efficient parallelization scheme,[28] it is possible to overcome the current time and scale limits of standard MD simulations while retaining a sufficiently high molecular resolution in the model to retain chemically resolved moieties. Past studies demonstrated the ability of this approach to investigate diverse soft matter systems, including lamellar and non-lamellar phospholipid moieties,[29–31] biocompatible block-copolymers,[32,33] non-charged surfactants,[34,35] and peptides.[36]

Recently, Zhu *et al.* introduced an efficient scheme based on the Ewald Summation to treat electrostatic interactions within hPF-MD.[37] In particular, the charged particles interact with an external electrostatic potential, derived from the charge density, similarly to the external potential based on the local density to evaluate the non-bonded interactions. Some of us reported a systematic study to tune the relative dielectric constant for the reproduction of structural properties of SDS surfactant aggregates in water and to check the stability of POPG bilayer in water.[38] This study showed that by an appropriate choice of the relative dielectric constant it is possible to reproduce the self-assembly process and stability of the aggregates (micellar or bilayer). An extension of the electrostatic treatment in the hPF-MD approach has been introduced by Bore et. al adopting a spatially resolved dielectric dependent on the local density fields of the different species.[39]

In this paper, we report the development of specific hybrid CG model for the biologically relevant Lipid A (hexa- and tetra-acyl chains). We show that the hPF-MD model not only reproduces the structural properties of atomistic simulations of hexa- and tetra-acylated Lipid A bilayers, but it also provides a representation of Lipid A phase diagram and vesicle aggregate structure highly consistent with experimental measurements *in vitro*.

2. Methods

2.1 The hPF-MD approach

In hPF-MD the total energy of the system is written as:

$$H = \sum_{m=1}^{N_{mol}} H_0(\{r\}_m) + W[\{\phi(r)\}] + W_{el}[\rho(r)], \quad 1$$

where $H_0(\{r\}_m)$ is the Hamiltonian of a single, non-interacting molecule $m, W[\{\phi(r)\}]$ is an interaction energy functional that depends on the particle density $\{\phi(r)\}$, and $W_{el}[\rho]$is the total electrostatic energy, dependent on the charge density ρ. We employ the functional form for $W[\phi(r)]$:

$$W[\{\phi(r)\}] = \frac{1}{2\phi_0} \int dr\, k_B T \sum_{K'} \chi_{KK'}\, \phi_K(r)\phi_{K'}(r) + \frac{1}{\kappa}(\sum_K \phi_K(r) - \phi_0))^2, \qquad (2)$$

as originally introduced.[25] Here k_B is the Boltzmann constant, T is the temperature of the system and $\phi_K(r)$ represents the coarse-grained number density of species K at position $\boldsymbol{r}$ and ϕ_0 is the total number density of the system. $\chi_{KK'}$ is the mixing energy term between species *K, K'*, and κ is a compressibility term regulating the local fluctuations of the density. Under this assumption, particles of a generic type *K* are subject to an external potential of the form [25]:

$$V_K(r) = \frac{\delta W}{\delta \phi(r)} = \frac{1}{\phi_0}(k_B T \sum_{K'} \chi_{KK'}\, \phi_{K'}(r) + \frac{1}{\kappa}(\sum_K \phi_K(r) - \phi_o)) \qquad (3)$$

The electrostatic energy of the system $W_{el}[\rho]$ is defined as:

$$W_{el}[\rho] = \frac{1}{2} \int dr\, \rho(r)\psi(r), \quad (4)$$

where the electrostatic potential $\psi$is governed by the Poisson equation:

$$-\nabla^2\psi(r) = \frac{\rho(r)}{\epsilon_r\epsilon_0} \qquad (5)$$

ϵ_r is the relative dielectric constant of the medium and ϵ_0 is the vacuum permittivity. The computation of $\psi(r)$ is performed using the recently developed adapted PME-approach as in references [37,38].

The calculation of the molecular forces is done by a particle-mesh approach where $\phi_K(r)s$ are computed on a grid, and their spatial derivatives estimated by finite difference. In the present work, the density gradients are calculated by a rotational invariant finite-difference stencil developed by Alfaraj *et al.*[40], as implemented for hPF-MD by Sevink *et al* [41]. A complete description of the hPF-MD method and its extension to electrostatics interactions is reported in refs.[25,37–39,42].

2.2 hPF-MD CG Model of Lipid A.

In this study, the single-molecule Hamiltonian $H_0(\{r\}_m)$ is based on a CG representation of both Lipid A, the ions, and the solvent (**Figure 1**). All intramolecular interactions have the same functional form as in standard force fields, [25] using the parameters developed in our previous studies,[29,37] apart from the length l_B between two L bead types. Specifically, we employ lengths l_B = 0.47 nm for hexa- and l_B = 0.34 nm for the tetra-acylated Lipid A in order to improve the agreement with the all atom structures. The complete list of Lipid A bonded parameters is reported in the Supporting Information.

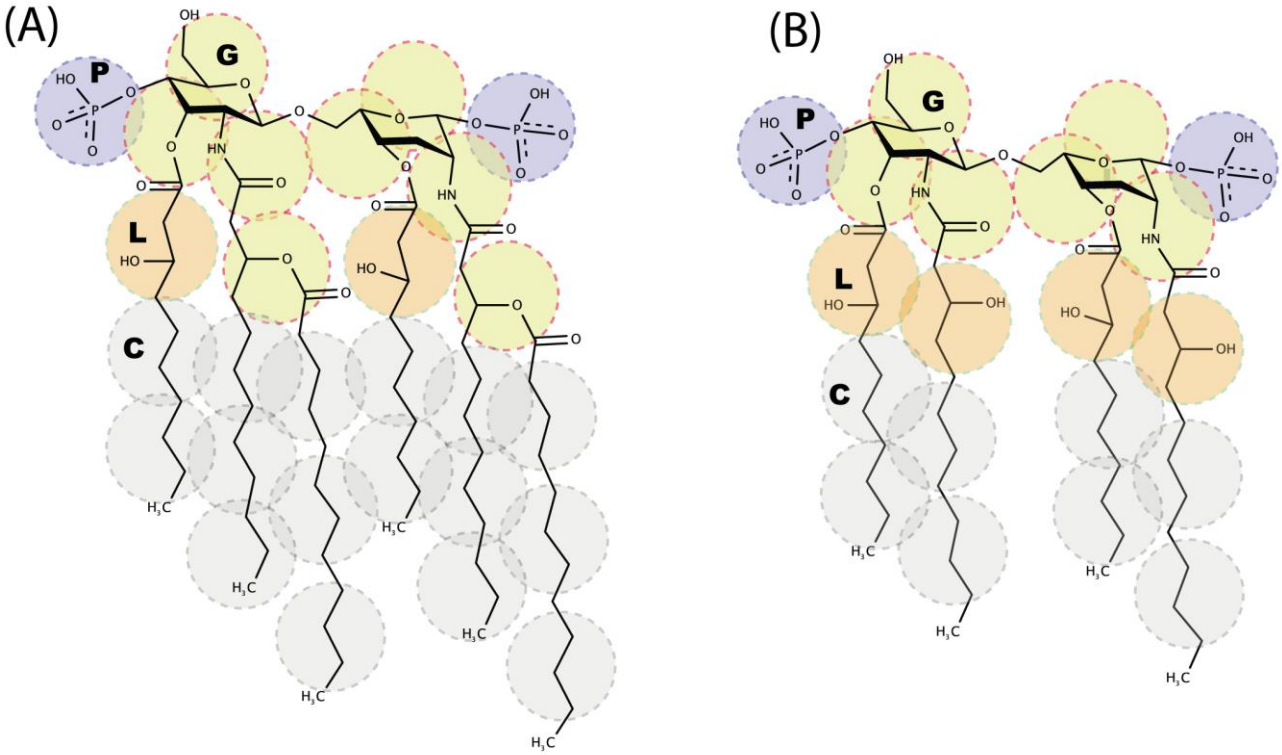

Figure 1. Chemical structures of (A) hexa- and (B) tetra-acylated forms of Lipid A. The drawings compare the atomic molecular structures and the corresponding coarse-grained mapping used in this work. The different bead types are indicated by the P, G, L, C letters, the same color in the circles indicates beads of the same type. The counter-ion bead (N), and the water CG bead (W), mapping four H_2O molecules, are not shown in the figure.

The $\chi_{KK'}$ parameters were first guessed by Flory-Huggins mixing parameters from the Martini force field Lennard-Jones binding energies,[43] and then further optimized to provide the best correspondence to all-atom reference data. The final $\chi_{KK'}$ parameters are reported in **Table 1** and were used in all simulations.

Table 1. Interaction matrix $\chi_{KK'} \times RT$ $(kJ\ mol^{-1})$ for the Lipid A/counter-ion/water system.

$\chi_{KK'} \times RT$	**L**	**P**	**G**	**C**	**N (Counter-ion)**	**W (Water)**
L	0	0	4.5	13.25	0	0
P	0	0	4.5	20	-7.2	-3.6
G	4.5	4.5	0	8.3	0	4.5
C	13.25	20	8.3	0	13.25	33.75

N (Counter-ion)	0	-7.2	0	13.25	0	0
W (Water)	0	-3.6	4.5	33.75	0	0

2.3 hPF-MD simulations of Lipid-A Membranes.

The initial CG structures of hexa- and tetra-acylated Lipid A bilayers were built starting from the corresponding all-atom models published in [19] (See **Scheme S1** in the Supporting Information). In particular, the area per lipid A_L for hexa- (1.53 nm^2) and tetra-acylated (1.2 nm^2) membrane systems is in agreement with experimental values.[44,45] The systems were neutralized by the addition of divalent cation beads randomly placed within a distance of 0.5 nm from the P beads in the Lipid A bilayer, and solvated by adding water beads using the Packmol package.[46] For the self-assembly simulations, the lipids were randomly distributed in the simulation box whereas for the vesicle simulation; the Packmol code was again used to build the initial geometry of the system.[46] The composition of all simulated systems is presented in **Table 2**.

hPF-MD simulations were performed using the OCCAM MD software.[42] A time step of 0.03 ps was used for all simulations. All simulations ran in the *NVT* ensemble with a temperature T = 300 K kept constant by the Andersen thermostat[47] with a collision frequency of 5 ps^{-1}. Simulations adopted a constant mesh size of l = 0.57 nm. The density field was updated every 100 time steps. Both the density update time and the mesh size were chosen to give good reproduction of the reference atomistic simulations, as reported in our previous works.[29,31–34]

2.4 Simulations of All-Atom Lipid A Membranes.

Benchmark all-atom MD simulations were performed for both the hexa- and tetra-acylated forms of Lipid A as previously described,[20] using an extension of the GROMOS 53A6 force field[20,48] in conjunction with the SPC water model.[49] MD simulations were performed in the *NPT* ensemble with a time step of 2.0 fs at 300 K and 1 bar. Bond lengths within the solute and the geometry of water molecules were constrained using the LINCS algorithm.[50] The temperatures of solute and

solvent were controlled by separately coupling them to a velocity rescaling thermostat with a relaxation time of 0.4 ps.[44] The pressure was maintained via the Berendsen pressure coupling algorithm with a semi-isotropic coordinate scaling coupling, coupling constant of 1 ps and an isothermal compressibility of 4.5×10^{-5} bar^{-1}.[45] Long-range electrostatic correction was applied using the Particle-Mesh Ewald (PME) approximation beyond a cut-off of 1.2 nm with a fourth order interpolation of charges on a 0.16 nm Fourier spacing. Nonbonded pair lists were updated every 5 steps using a single cut-off scheme for atom pairs beyond a cut-off of 1.2 nm. The systems were first equilibrated for 100 ns to converge the area per lipid molecule, subsequent data production was performed for additional 400 ns. All-atom simulations were performed using the GROMACS 4.5.4 software suite.[51]

Table 2. Composition of the system simulated in this work.

System	**Method**	**Lipid A molecules (Hexa-acyl)**	**Lipid A molecules (Tetra-acyl)**	**Counter ions**	**W beads**	**Box size** *(x,y,z)* [nm^3]	**Time** [ns]
HPF1	hPF-MD	256	-	256 N^{2+}	9556	14.45 x 13.34 x 9.19	300
HPF2	hPF-MD	256	-	512 N^{+}	9483	14.08 x 12.99 x 9.35	300
HPF3	hPF-MD	-	128	256 N^{2+}	4125	13.62 x 5.33 x 7.86	300
HPF4	hPF-MD	1200	-	1200 N^{2+}	70000	22.0 x 22.0 x 22.0	4200
HPF5	hPF-MD	1400	-	1400 N^{2+}	15000	17.0 x 17.0 x 17.0	3550
HPF6	hPF-MD	644	-	644 N^{2+}	221235	30.0 x 30.0 x 30.0	1200
AA1	All-atom	128	-	128 Ca_2^{+}	4518	13.47 x 7.30 x 9.02	400
AA2	All-atom	128	-	256 Na^{+}	4474	13.71 x 5.36 x 8.00	400

3. Results

Effect of the dielectric constant ϵ_r on the stability of Lipid A bilayer. Appropriate calibration of the effective dielectric constant ϵ_r is fundamental for the correct description of charged lipid bilayers, as demonstrated by past work on a POPG membrane.[38] For this reason, we first investigated the

dependency of the stability of Lipid A bilayers as a function of different values of the relative dielectric constant.

Starting from an initial CG configuration of hexa-acylated Lipid A mapped on the reference atomistic configuration (HPF1, **Table 2**), we ran four hPF-MD simulations, each 300 ns long, at $\epsilon_r = 1, 5, 15, 80$ values, reporting the corresponding average structures and density profiles for the different chemical moieties along the direction normal to the plane of the bilayer in **Figure 2**.

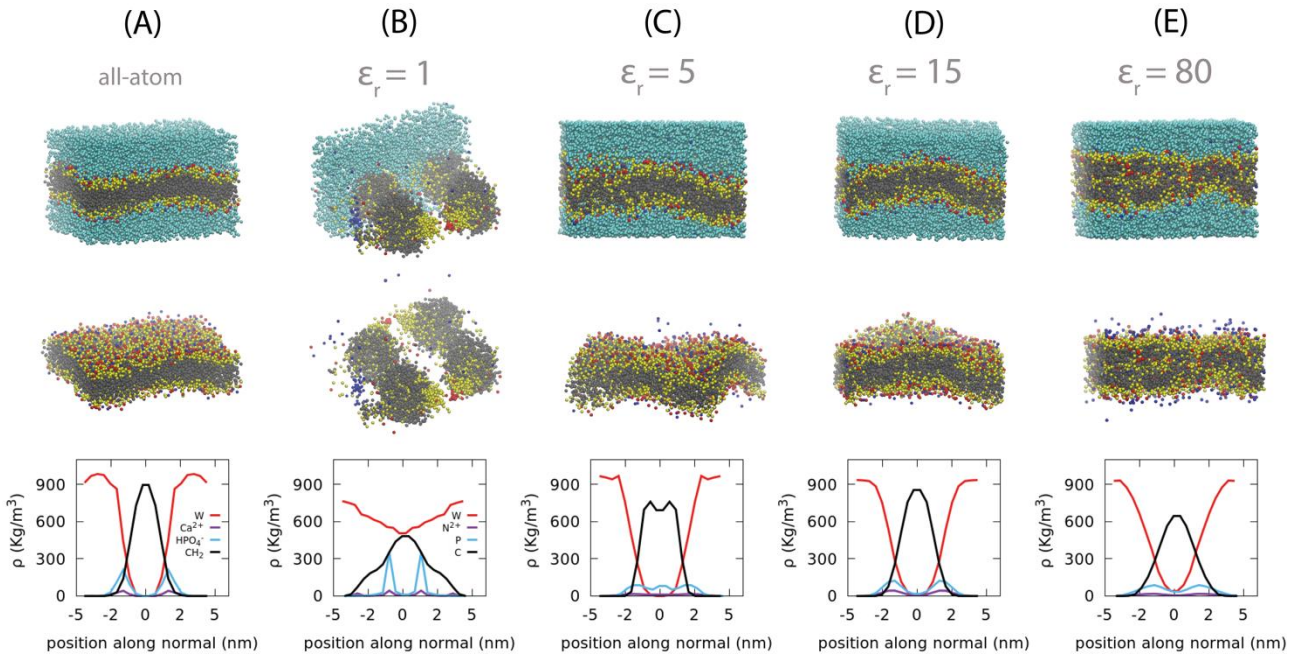

Figure 2. **Equilibrated structures of Lipid A bilayers.** *Top panels:* Representative snapshots of the equilibrium configurations for (A) all-atom and (B-E) hPF-MD simulations of hexa-acylated Lipid A using different relative dielectric constant (ϵ_r)values. The CG bead types are colored as: P (red), G and L (yellow), C (gray), N^{2+} (blue), and W (cyan). The same configuration is also represented without the water beads for the sake of clarity. *Bottom panels:* Average mass density profiles for the corresponding systems shown above.

As expected, the organization of the Lipid A layers depends on the value of the dielectric constant (**Figure 2)**. A very low value (ϵ_r = 1) produces an unstable bilayer with complete disruption of the bilayer structure within the first 30 ns of simulation, while larger values of ϵ_r maintain the global lamellar structure of the membrane. hPF-MD simulations using a value of ϵ_r = 15 (**Figure 2D**) yield a stable bilayer structure within the simulation time scale and reproduces the most accurately the density profiles of the atomistic reference. Conversely, the density profiles indicate that the

organization of Lipid A inside the membrane is not correct for ϵ_r = 5 and 80. In both cases we observe the appearance of strong surface undulation and a migration of the hydrophilic sites to the middle plane of the bilayer (see snapshots with ϵ_r = 80), with the negatively charged P beads being distributed along the whole cross-section of the membrane (**Figures 2C,E**), indicating that the lipids are tilted by an angle greater than 45 degrees (**Figure 2E)**.

Comparison of the calculated density profiles for the all-atom reference (AA1, **Table 2**) and the hPF-MD simulations at ϵ_r = 15 further substantiates semi-qualitative agreement between the two models (**Figure 3**). In particular, data from the two sets of simulations agree well for the symmetric distribution of the peaks, the bilayer thickness D_{HH} measured as the distance between P-P sites (3.82 nm for the reference system and 3.74 nm in hPF-MD), and for the location of the phosphate groups in the bilayer and the distribution of the acyl tails. The hPF-MD density profiles show a slightly broader width than the all-atom reference. This is consistent with what has been previously reported for other lipid bilayers and is connected to the softness of the potential employed in the hPF model. The biggest discrepancy between hPF-MD and all-atom models is in the broader distribution of the N^{2+} counterions in the hPF-MD model compared to the all-atom Ca^{2+} ones, and their penetration into the lipophilic region of the bilayer (**Figure 4**). Similar behavior for the ions was previously reported for the DOPG membrane,[38] and can be attributed to both the soft nature of the hPF-MD potentials and the lack of an explicit change in the dielectric environment between the solvent and lipid phases.

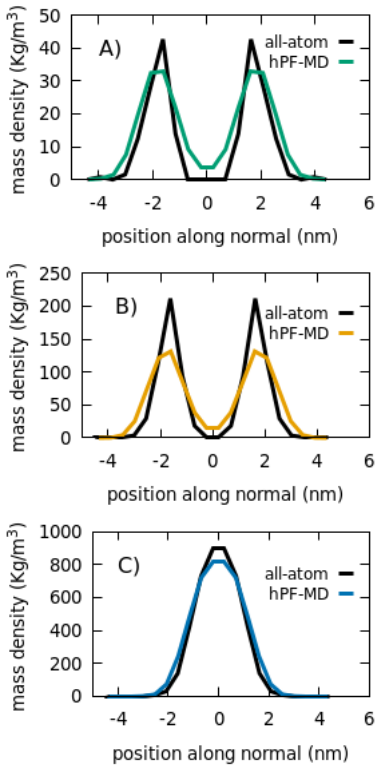

Figure 3. Comparison of density profiles for the hexa-acylated Lipid-A HPF-MD simulation $\epsilon_r = 15$ against the reference atomistic simulation: (A) Ca^{2+}/N, (B)HPO_4^-/P, and (C) CH_2/C moieties.

Effect of counterion valence on the bilayer structure. It was previously shown that divalent cations induce considerable changes in the physico-chemical parameters of LPS membranes such as hydration, acyl chain mobility, and aggregation state compared to monovalent cations.[7,52,53] Divalent cations increase the liquid-crystal transition temperature (T_c) values and acyl chain order, whereas Na^+ increases the hydration of the LPS leaflet.[3,7,54–56] Therefore, we investigated how well the hPF-MD model reproduces the effect of divalent versus mono-valent counterions on the stability and hydration of the hexa-acylated Lipid A membrane (HPF2, **Table 2**).

In the present hPF-MD model the only difference in the parameters of the mono- (N^+) and divalent (N^{2+}) counterions is the bead charge. Yet, the replacement of one N^{2+} by two N^+ particles led to a striking structural rearrangement of the bilayer, with the system of N^+ showing a persistent undulated configuration (**Figure 4**). This behavior is consistent with atomistic simulations of Lipid-A bilayers which have shown that Na^+ cations induce a significantly higher degree of disorder compared to Ca^{2+}

(AA2, **Table 2**).[7] In particular, Pontes *et al.* speculated that the non-lamellar arrangement of Lipid-A induced by replacement of Ca^{2+} by Na^{+} is reminiscent, given the limited time and length scales reachable by atomistic models, of an inverted hexagonal H_{II} phase.[7] Indeed, LPS exhibits a rather complex structural polymorphism with a strong dependence of the supramolecular aggregate structure on ambient conditions, and Lipid A has been shown to preferentially form non-lamellar structures under physiological conditions.[11,54,57]

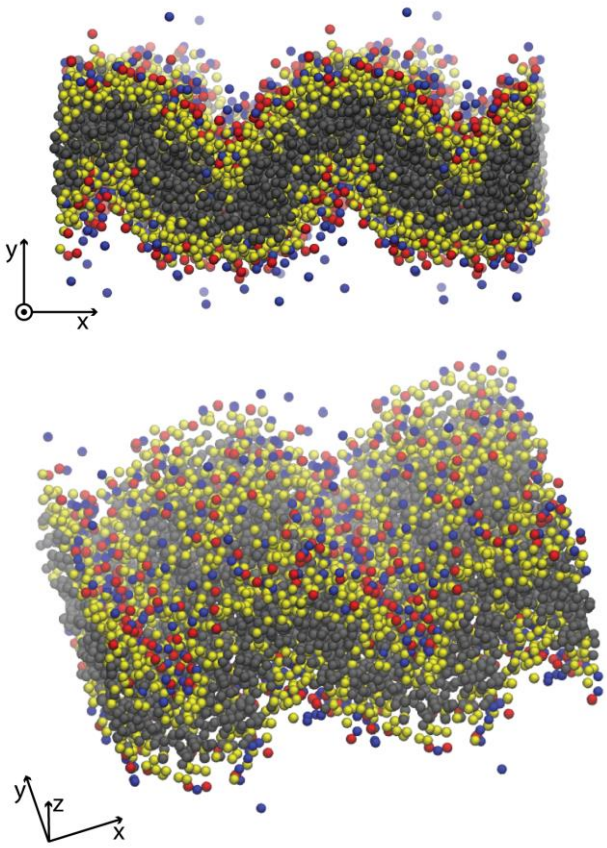

Figure 4. Structure of hexa-acylated Lipid A bilayer in the presence N^{+} counterions. Color code: N^{+} (blue), G/L (yellow), P (red) and C (gray). Water CG beads are not explicitly reported for clarity.

Transferability of χ parameters: hPF-MD simulations of tetra-acylated Lipid A. The length and the number of hydrophobic chains of Lipid A varies along different species (*e.g. Escherichia coli*, *Pseudomonas aeruginosa*, *Salmonella minnesota*). In order to assess if intermolecular interaction parameters obtained from the parameterization of the hexa-acylated Lipid A (Table 1) are transferable

to the tetra-acylated one, we performed hPF-MD simulations for the latter system using N^{2+} counterions and a dielectric constant $\epsilon_r = 15$ (HPF3, **Table 2**).

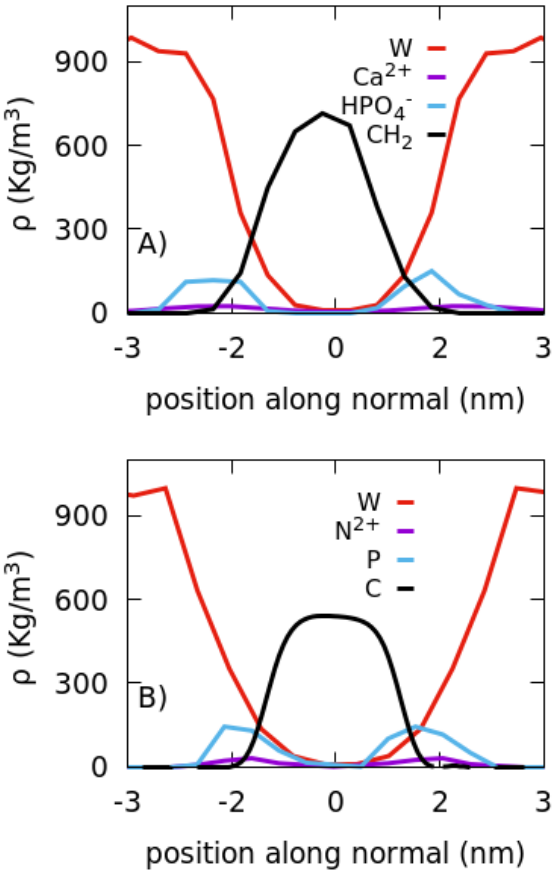

Figure 5. Mass density profile calculated along the normal direction of the tetra-acylated Lipid-A membrane plane for: A) reference tetra-acylated Lipid-A bilayer, B) HPF-MD simulation with ϵ_r = 15. The profiles from HPF-MD simulation were calculated by averaging the last 50 ns of trajectory. The PO_4^{2-} curve corresponds to site P (purple), CH_2 corresponds to C site (yellow) and the Ca_2^+ corresponds to site N (blue). The water site (W) curve is shown in red.

Comparison between density profiles from all-atom (AA3, **Table 2**) and hPF-MD simulations show that the corresponding peak positions of the hPF-MD curves are consistent with those in the reference atomistic simulation (**Figure 5**), apart from the appearance of less pronounced profiles than those of the reference all-atom model, typical of such a modelling approach. This supports the transferability of the χ parameters between different Lipid A structures (e.g. number, length and position of acyl chains).

***Self-Assembly of the Lamellar Phase*.** The present results indicate that the proposed model reproduces with good accuracy the all-atom structural properties of pre-equilibrated Lipid A bilayers. To further validate our model, we verified its ability in describing the self-assembly of the hexa-acylated Lipid A/N^{2+} in water. We studied two different concentrations (70 and 30 $\%_{w/w}$ of water content, HPF4 and HPF5, **Table 2**) that, according to the experimental phase diagram, would produce significantly different stable assemblies. In particular, at the lower concentration value (70 % water) Lipid A should aggregate in a lamellar/cubic phase (L+Q), while the higher concentration (30 % water) would produce a lamellar/hexagonal (L+H) state.

The time evolution of the self-assembly processes, starting from random mixtures of Lipid A/water, is reported in **Figure 6**. The system with 70% w/w of water goes through an initial chaotic aggregation, followed by the formation of a bilayer structure around 1 μs of MD, finally reaching a stable conformation after 2.8 μs (**Figure 6A**). The equilibrium conformation of the assembly shows a coexistence of two phases made of a planar bilayer (lamellar phase) fused with a cylindrical micelle (cubic phase), in agreement with the experimental phase diagram.[11,52] The system with lower content of water (30 % w/w), reaches an equilibrium conformation after 1 μs. In this case, the self-assembled structure shows interconnected lamellae organised in an irregular honey-comb-like pattern (**Figure 6B**). This finding is also consistent with the (L+Q) aggregation evidenced in the experiment. The ability of hPF-MD simulations to describe very different aggregation states indicates that the model has adequate transferability to respond to external conditions. In particular, the proposed model is able to describe surfaces with different curvature radii, as highlighted in **Figure 6C,** where two sections (lateral and perpendicular) of the equilibrium conformation of the system with 70 % of water are reported.

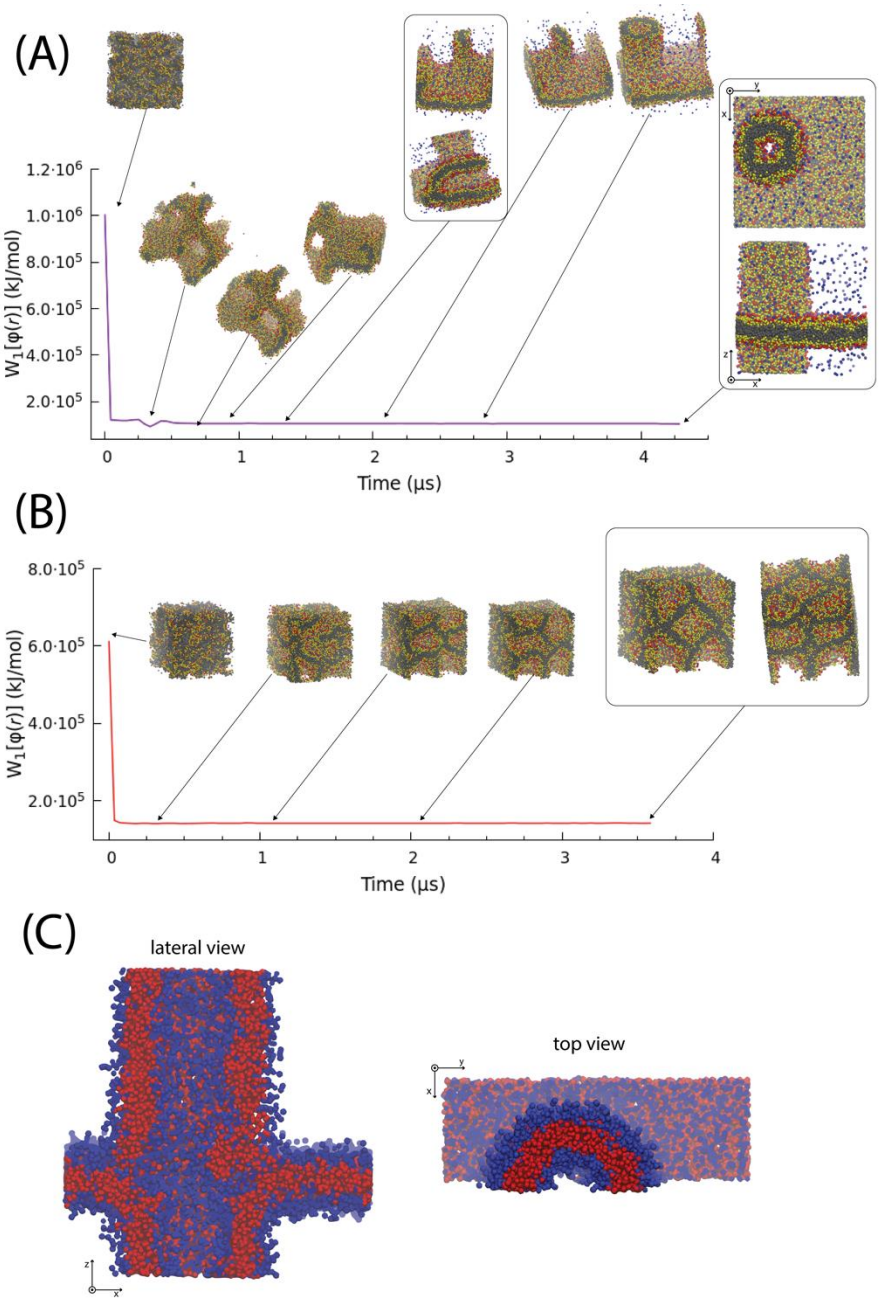

Figure 6. Time evolution of the $W_1[\{\phi(r)\}]$ potential for hexa-acylated Lipid A/water mixture (where $W_1[\{\phi(r)\}] = \frac{1}{2\phi_0}\int dr\, k_B T \sum_{K'} \chi_{KK'}\, \phi_K(r)\phi_{K'}(r)$ is the first term of the eq. 2): (A) 70% w/w of water, (B) 30% w/w of water. Representative snapshots are reported in plot. The color code used in the reported snapshots is the same used as in Figure 4. Water beads are not reported for clarity. Both simulations have been performed at 313 K. C) Lateral and top view of the equilibrium assembly of 70% w/w system. To enhance the contrast, Lipid A head beads are reported in blue, while hydrophobic tails are reported in red. Ions and water beads are not reported for clarity.

Lipid A Vesicle. As a final inspection on the aggregation of Lipid A, we investigated the structure of non-periodic vesicles in water. The vesicle consisted of 204 hexa-acylated Lipid A in the inner layer

and 440 in the outer layer with a diameter of 15 nm (HPF6, **Table 2**) with an equal number of N^{2+} counterions placed close to the P beads in both layers. The time evolution of the radius of the vesicle, interaction potentials and representative snapshots of the vesicle conformation indicate that the vesicle was stable within the simulated time (**Figure 8**). After the initial relaxation during the first 10 ns of the simulation, the vesicle retained a mostly spherical shape with a radius of ~7.7 nm (**Figure 8B)**. Deviations from ideal sphericity are attributed to the non-stoichiometric binding of counterions in the outer layer, which reflect into local, instantaneous strong repulsion between the phosphorylated heads. As a consequence, the effective head area for the different molecules constituting the vesicle is instantaneously very different, producing structural deformations in the assembly. These findings indicate that liposome-like aggregates of hexa-acetylated Lipid A are stable, opening the way to investigations of how Lipid A activates proteins involved in the immune response of hosts.

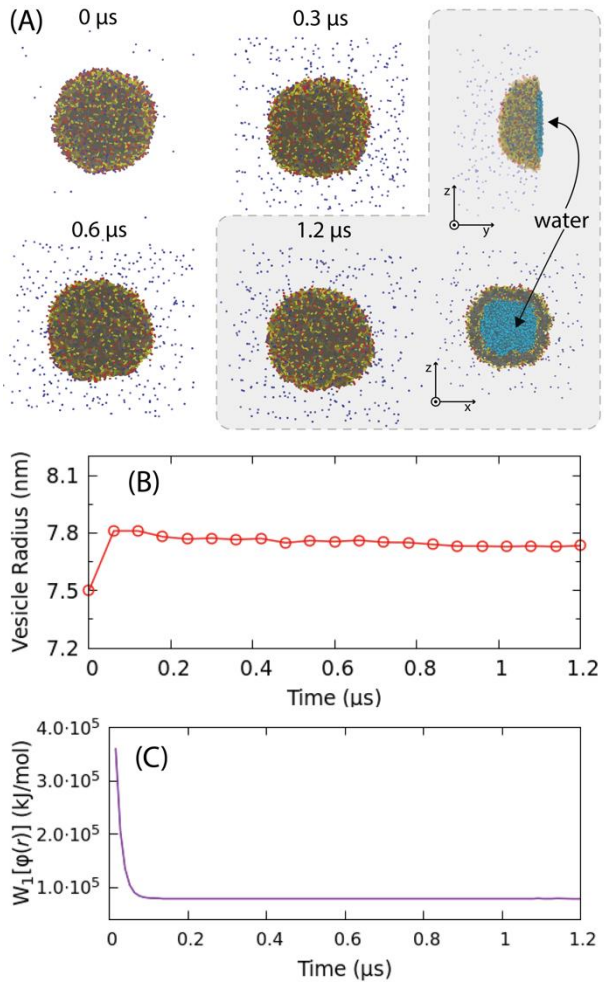

Figure 8. (A) Snapshots of Lipid A vesicle at different simulation times. For the last snapshot (at 1.2 μs) two sections of the vesicle with the water inside its internal cavity are reported. For clarity the water beads outside the vesicle are omitted. The bead types are reported by following the same color code used in Figure 2. (B) Radius of the vesicle as a function of time. (C) Time evolution of the $W_1[\{\phi(r)\}]$ potential.

Conclusion

We presented a hPF-MD model for Lipid A that not only reproduces the structural properties of atomistic simulations but provides an experimentally-consistent description of the phase diagram of this complex glycolipid. The underlying molecular model employs a CG mapping similar to that of the Martini force-field, and most importantly, explicit electrostatic interactions to accurately treat interaction with mono and divalent counterions. The optimized set of parameters reproduce the lamellar phase of reference all-atom models of constituted Lipid A bilayers with good qualitative and

quantitative performance for structural properties such as bilayer thickness, area per lipid, and density profiles.

The interaction parameters are transferable through chemical variants of Lipid A. Specifically, we verified the ability of reproducing the assembly of both hexa- and tetra-acylated Lipid A, as well as global structural modification induced by the presence of monovalent instead of divalent counterions. Our model is also able to predict the self-assembly of Lipid A, and the spontaneous formation of complex L+Q, or L+H phases as a function of the water/lipid concentration ratio. In particular, we observed the formation of complex structures indicating the coexistence of such phases and in agreement with the experimental phase diagram. The proposed model is able to describe surfaces with different radii of curvature going from the infinite radius (planar bilayer) to finite radii (inverted hexagonal and cubic assemblies). The stability of a Lipid A vesicle, starting from a pre-assembled configuration, has been also investigated, finding that our parameterization maintains a stable and spherical vesicle in over 1 μs of simulation time.

The optimized relative dielectric constant provides a proper description of the electrostatic interactions, which are the fundamental ingredient to correctly describe complex system such as Lipid A aggregates. These promising results encourage the investigation of more complex lipopolysaccharide systems of major relevance for bio-medical studies.

Acknowledgement

GM and ADN wish to thank the HPC team of Enea (http:// www.enea.it) for using the ENEA-GRID and the HPC facilities CRESCO (http://www.cresco.enea.it) in Portici. C.M.

SLB and MC acknowledge the support of the Research Council of Norway through the CoE Hylleraas Centre for Quantum Molecular Sciences (Grant No. 262695).

References

[1] H. Nikaido, Molecular Basis of Bacterial Outer Membrane Permeability Revisited, Microbiol.

Mol. Biol. Rev. 67 (2003) 593–656. doi:10.1128/MMBR.67.4.593–656.2003.

[2] S.G. Wilkinson, Bacterial lipopolysaccharides—Themes and variations, Prog. Lipid Res. 35 (1996) 283–343. doi:https://doi.org/10.1016/S0163-7827(96)00004-5.

[3] N. Kućerka, E. Papp-Szabo, M.P. Nieh, T.A. Harroun, S.R. Schooling, J. Pencer, E.A. Nicholson, T.J. Beveridge, J. Katsaras, Effect of cations on the structure of bilayers formed by lipopolysaccharides isolated from Pseudomonas aeruginosa PAO1, J. Phys. Chem. B. 112 (2008) 8057–8062. doi:10.1021/jp8027963.

[4] M. Caroff, D. Karibian, Structure of bacterial lipopolysaccharides, Carbohydr. Res. 338 (2003) 2431–2447. doi:https://doi.org/10.1016/j.carres.2003.07.010.

[5] H. Ma, F.J. Irudayanathan, W. Jiang, S. Nangia, Simulating Gram-Negative Bacterial Outer Membrane: A Coarse Grain Model, J. Phys. Chem. B. 119 (2015) 14668–14682. doi:10.1021/acs.jpcb.5b07122.

[6] A. Molinaro, O. Holst, F. Di Lorenzo, M. Callaghan, A. Nurisso, G. D'Errico, A. Zamyatina, F. Peri, R. Berisio, R. Jerala, J. Jiménez-Barbero, A. Silipo, S. Martín-Santamarí, Chemistry of lipid a: At the heart of innate immunity, Chem. - A Eur. J. 21 (2015) 500–519. doi:10.1002/chem.201403923.

[7] F.J.S. Pontes, V.H. Rusu, T.A. Soares, R.D. Lins, The effect of temperature, cations, and number of Acyl chains on the lamellar to non-lamellar transition in Lipid-A membranes: A microscopic view, J. Chem. Theory Comput. 8 (2012) 3830–3838. doi:10.1021/ct300084v.

[8] A.B. Schromm, K. Brandenburg, H. Loppnow, A.P. Moran, M.H.J. Koch, E.T.H. Rietschel, U. Seydel, Biological activities of lipopolysaccharides are determined by the shape of their lipid A portion, Eur. J. Biochem. 267 (2000) 2008–2013. doi:10.1046/j.1432-1327.2000.01204.x.

[9] K. Brandenburg, U. Seydel, A.B. Schromm, H. Loppnow, M.H.J. Koch, E.T. Rietschel, Conformation of lipid A, the endotoxic center of bacterial lipopolysaccharide, Innate

Immun. 3 (1996) 173–178. doi:10.1177/096805199600300302.

[10] S.I. Miller, R.K. Ernst, M.W. Bader, LPS, TLR4 and infectious disease diversity, Nat. Rev. Microbiol. 3 (2005) 36–46. doi:10.1038/nrmicro1068.

[11] K. Brandenburg, M.H.J.H.J. Koch, U. Seydel, Phase diagram of deep rough mutant lipopolysaccharide from Salmonella minnesota R595, J. Struct. Biol. 108 (1992) 93–106. doi:10.1016/1047-8477(92)90010-8.

[12] H. Reichelt, C.A. Faunce, H.H. Paradies, The phase diagram of charged colloidal lipid A-diphosphate dispersions, J. Phys. Chem. B. 112 (2008) 3290–3293. doi:10.1021/jp711720j.

[13] S. Khalid, T.J. Piggot, F. Samsudin, Atomistic and Coarse Grain Simulations of the Cell Envelope of Gram-Negative Bacteria: What Have We Learned?, Acc. Chem. Res. 52 (2019) 180–188. doi:10.1021/acs.accounts.8b00377.

[14] R.D. Lins, T.P. Straatsma, Computer simulation of the rough lipopolysaccharide membrane of Pseudomonas aeruginosa, Biophys. J. 81 (2001) 1037–1046. doi:10.1016/S0006-3495(01)75761-X.

[15] K.N. Kirschner, R.D. Lins, A. Maass, T.A. Soares, A glycam-based force field for simulations of lipopolysaccharide membranes: Parametrization and validation, J. Chem. Theory Comput. 8 (2012) 4719–4731. doi:10.1021/ct300534j.

[16] T.A. Soares, T.P. Straatsma, Assessment of the convergence of molecular dynamics simulations of lipopolysaccharide membranes, Mol. Simul. 34 (2008) 295–307. doi:10.1080/08927020701829880.

[17] A. Li, J.W. Schertzer, X. Yong, Molecular dynamics modeling of Pseudomonas aeruginosa outer membranes, Phys. Chem. Chem. Phys. 20 (2018) 23635–23648. doi:10.1039/c8cp04278k.

[18] E.L. Wu, O. Engström, S. Jo, D. Stuhlsatz, M.S. Yeom, J.B. Klauda, G. Widmalm, W. Im,

Molecular dynamics and NMR spectroscopy studies of E. coli lipopolysaccharide structure and dynamics, Biophys. J. 105 (2013) 1444–1455. doi:10.1016/j.bpj.2013.08.002.

[19] D.E.S.S. Santos, L. Pol-Fachin, R.D. Lins, T.A. Soares, Polymyxin Binding to the Bacterial Outer Membrane Reveals Cation Displacement and Increasing Membrane Curvature in Susceptible but Not in Resistant Lipopolysaccharide Chemotypes, J. Chem. Inf. Model. 57 (2017) 2181–2193. doi:10.1021/acs.jcim.7b00271.

[20] V.H. Rusu, R. Baron, R.D. Lins, PITOMBA: Parameter interface for oligosaccharide molecules based on atoms, J. Chem. Theory Comput. 10 (2014) 5068–5080. doi:10.1021/ct500455u.

[21] B. Van Oosten, T.A. Harroun, A MARTINI extension for Pseudomonas aeruginosa PAO1 lipopolysaccharide, J. Mol. Graph. Model. 63 (2016) 125–133. doi:10.1016/j.jmgm.2015.12.002.

[22] P.C. Hsu, B.M.H. Bruininks, D. Jefferies, P. Cesar Telles de Souza, J. Lee, D.S. Patel, S.J. Marrink, Y. Qi, S. Khalid, W. Im, CHARMM-GUI Martini Maker for modeling and simulation of complex bacterial membranes with lipopolysaccharides, J. Comput. Chem. 38 (2017). doi:10.1002/jcc.24895.

[23] F.A. Baltoumas, S.J. Hamodrakas, V.A. Iconomidou, The gram-negative outer membrane modeler: Automated building of lipopolysaccharide-rich bacterial outer membranes in four force fields, J. Comput. Chem. 40 (2019) 1727–1734. doi:10.1002/jcc.25823.

[24] T Kawakatsu., Statistical physics of polymers: an introduction. Springer-Verlag, Berlin, Heidelberg, 2004. ISBN 3-540-43440-2. pp 216, Polym. Int. (2005). doi:10.1002/pi.1772.

[25] G. Milano, T. Kawakatsu, Hybrid particle-field molecular dynamics simulations for dense polymer systems., J. Chem. Phys. 130 (2009) 214106. doi:10.1063/1.3142103.

[26] T.A. Soares, S. Vanni, G. Milano, M. Cascella, Toward Chemically Resolved Computer Simulations of Dynamics and Remodeling of Biological Membranes, J. Phys. Chem. Lett. 8

(2017) 3586–3594. doi:10.1021/acs.jpclett.7b00493.

[27] S. J. Marrink, V. Corradi, P. C.T. Souza, H. I. Ingólfsson, D. Peter Tieleman, M. S.P. Sansom, S.J. Marrink, P.C.T. Souza, V. Corradi, D.P. Tieleman, H.I. Ingólfsson, M.S.P. Sansom, Computational Modeling of Realistic Cell Membranes, Chem. Rev. 119 (2019) 6184–6226. doi:10.1021/acs.chemrev.8b00460.

[28] Y. Zhao, A. De Nicola, T. Kawakatsu, G. Milano, Hybrid particle-field molecular dynamics simulations: Parallelization and benchmarks, J. Comput. Chem. 33 (2012) 868–880. doi:10.1002/jcc.22883.

[29] A. De Nicola, Y. Zhao, T. Kawakatsu, D. Roccatano, G. Milano, Hybrid Particle-Field Coarse-Grained Models for Biological Phospholipids, J. Chem. Theory Comput. 7 (2011) 2947–2962. doi:10.1021/ct200132n.

[30] A. De Nicola, Y. Zhao, T. Kawakatsu, D. Roccatano, G. Milano, Validation of a hybrid MD-SCF coarse-grained model for DPPC in non-lamellar phases, Theor. Chem. Acc. 131 (2012) 1167. doi:10.1007/s00214-012-1167-1.

[31] E. Sarukhanyan, A. De Nicola, D. Roccatano, T. Kawakatsu, G. Milano, A. De Nicola, D. Roccatano, T. Kawakatsu, G. Milano, Spontaneous insertion of carbon nanotube bundles inside biomembranes: A hybrid particle-field coarse-grained molecular dynamics study, Chem. Phys. Lett. 595–596 (2014) 156–166. doi:10.1016/j.cplett.2014.01.057.

[32] A. De Nicola, T. Kawakatsu, G. Milano, A Hybrid Particle-Field Coarse-Grained Molecular Model for Pluronics Water Mixtures, Macromol. Chem. Phys. 214 (2013) 1940–1950. doi:10.1002/macp.201300214.

[33] A. De Nicola, S. Hezaveh, Y. Zhao, T. Kawakatsu, D. Roccatano, G. Milano, Micellar drug nanocarriers and biomembranes: how do they interact?, Phys. Chem. Chem. Phys. 16 (2014) 5093. doi:10.1039/c3cp54242d.

[34] A. De Nicola, T. Kawakatsu, C. Rosano, M. Celino, M. Rocco, G. Milano, Self-Assembly of Triton X-100 in Water Solutions: A Multiscale Simulation Study Linking Mesoscale to Atomistic Models, J. Chem. Theory Comput. 11 (2015) 4959–4971. doi:10.1021/acs.jctc.5b00485.

[35] A. Pizzirusso, A. De Nicola, G.J.A. Sevink, A. Correa, M. Cascella, T. Kawakatsu, M. Rocco, Y. Zhao, M. Celino, G. Milano, Biomembrane solubilization mechanism by Triton X-100: a computational study of the three stage model, Phys. Chem. Chem. Phys. 19 (2017) 29780–29794. doi:10.1039/C7CP03871B.

[36] S.L. Bore, G. Milano, M. Cascella, Hybrid Particle-Field Model for Conformational Dynamics of Peptide Chains, J. Chem. Theory Comput. 14 (2018) 1120–1130. doi:10.1021/acs.jctc.7b01160.

[37] Y.-L. Zhu, Z.-Y. Lu, G. Milano, A.-C. Shi, Z.-Y. Sun, Hybrid particle–field molecular dynamics simulation for polyelectrolyte systems, Phys. Chem. Chem. Phys. 18 (2016) 9799–9808. doi:10.1039/C5CP06856H.

[38] H.B. Kolli, A. De Nicola, S.L. Bore, K. Schäfer, G. Diezemann, J. Gauss, T. Kawakatsu, Z. Lu, Y.-L.Y. Zhu, G. Milano, M. Cascella, Hybrid Particle-Field Molecular Dynamics Simulations of Charged Amphiphiles in an Aqueous Environment, J. Chem. Theory Comput. 14 (2018) 4928–4937. doi:10.1021/acs.jctc.8b00466.

[39] S.L. Bore, H.B. Kolli, T. Kawakatsu, G. Milano, M. Cascella, Mesoscale Electrostatics Driving Particle Dynamics in Nonhomogeneous Dielectrics, J. Chem. Theory Comput. 15 (2019) 2033–2041. doi:10.1021/acs.jctc.8b01201.

[40] M. Alfaraj, Y. Wang, Y. Luo, Enhanced isotropic gradient operator, Geophys. Prospect. 62 (2014) 507–517. doi:10.1111/1365-2478.12106.

[41] G.J.A. Sevink, F. Schmid, T. Kawakatsu, G. Milano, Combining cell-based hydrodynamics with

hybrid particle-field simulations: efficient and realistic simulation of structuring dynamics, Soft Matter. 13 (2017) 1594–1623. doi:10.1039/c6sm02252a.

[42] Y. Zhao, A. De Nicola, T. Kawakatsu, G. Milano, Parallelization and benchmark, J. Comput. Chem. 33 (2012) 868–880.

[43] S.J. Marrink, H.J. Risselada, S. Yefimov, D.P. Tieleman, A.H. De Vries, The MARTINI force field: Coarse grained model for biomolecular simulations, J. Phys. Chem. B. 111 (2007) 7812–7824. doi:10.1021/jp071097f.

[44] G. Bussi, D. Donadio, M. Parrinello, Canonical sampling through velocity rescaling, J. Chem. Phys. 126 (2007) 14101. doi:10.1063/1.2408420.

[45] H.J.C. Berendsen, J.P.M. Postma, W.F. van Gunsteren, A. DiNola, J.R. Haak, Molecular dynamics with coupling to an external bath, J. Chem. Phys. 81 (1984) 3684–3690. doi:10.1063/1.448118.

[46] L. Martínez, R. Andrade, E.G. Birgin, J.M. Martínez, Software News and Update Packmol: A Package for Building Initial Configurations for Molecular Dynamics Simulations, J. Comput. Chem. 30 (2009) 2157–2164.

[47] H.C. Andersen, Molecular dynamics simulations at constant pressure and/or temperature, J. Chem. Phys. 72 (1980) 2384–2393. doi:10.1063/1.439486.

[48] L. Pol-Fachin, V.H. Rusu, H. Verli, R.D. Lins, GROMOS 53A6 GLYC, an improved GROMOS force field for hexopyranose-based carbohydrates, J. Chem. Theory Comput. (2012). doi:10.1021/ct300479h.

[49] H. J. C. Berendsen, J. R. Grigera, T. P. Straatsma, The missing term in effective pair potentials, J. Phys. Chem. 91 (2002) 6269–6271. doi:10.1021/j100308a038.

[50] B. Hess, H. Bekker, H.J.C. Berendsen, J.G.E.M. Fraaije, LINCS: A linear constraint solver for molecular simulations, J. Comput. Chem. 18 (1997) 1463–1472. doi:10.1002/(SICI)1096-

987X(199709)18:12<1463::AID-JCC4>3.0.CO;2-H.

[51] B. Hess, C. Kutzner, D. van der Spoel, E. Lindahl, GROMACS 4: Algorithms for Highly Efficient, Load-Balanced, and Scalable Molecular Simulation, J. Chem. Theory Comput. 4 (2008) 435–447. doi:10.1021/ct700301q.

[52] K. Brandenburg, M.H.J. Koch, U. Seydel, Phase diagram of lipid A from Salmonella minnesota and Escherichia coli rough mutant lipopolysaccharide, J. Struct. Biol. 105 (1990) 11–21. doi:10.1016/1047-8477(90)90093-R.

[53] S. Snyder, D. Kim, T. J. McIntosh, T.J. McIntosh, Lipopolysaccharide Bilayer Structure: Effect of Chemotype, Core Mutations, Divalent Cations, and Temperature, Biochemistry. 38 (1999) 10758–10767. doi:10.1021/bi990867d.

[54] P. Garidel, M. Rappolt, A.B. Schromm, J. Howe, K. Lohner, J. Andrä, M.H.J. Koch, K. Brandenburg, Divalent cations affect chain mobility and aggregate structure of lipopolysaccharide from Salmonella minnesota reflected in a decrease of its biological activity, Biochim. Biophys. Acta - Biomembr. 1715 (2005) 122–131. doi:10.1016/j.bbamem.2005.07.013.

[55] C. Jeworrek, F. Evers, J. Howe, K. Brandenburg, M. Tolan, R. Winter, Effects of specific versus nonspecific ionic interactions on the structure and lateral organization of lipopolysaccharides, Biophys. J. 100 (2011) 2169–2177. doi:10.1016/j.bpj.2011.03.019.

[56] A. Nascimento, F.J.S. Pontes, R.D. Lins, T.A. Soares, Hydration, ionic valence and cross-linking propensities of cations determine the stability of lipopolysaccharide (LPS) membranes, Chem. Commun. 50 (2014) 231–233. doi:10.1039/c3cc46918b.

[57] K. Brandenburg, W. Richter, M.H.. Koch, H.. Meyer, U. Seydel, Characterization of the nonlamellar cubic and HII structures of lipid A from Salmonella enterica serovar Minnesota by X-ray diffraction and freeze-fracture electron microscopy, Chem. Phys. Lipids. 91 (1998)

53–69. doi:10.1016/S0009-3084(97)00093-5.